Structural and FT-IR studies of phenolic 2,8-dihydroxy-7H-furo [2,3-f]chromen-7-one derivative isolated from *Tibouchina paratropica*

María I. Tracanna[1], Elida Romano[2], Ana B. Raschi[2], Antonio M. Fortuna[3], Silvia Antonia Brandán[2,*]

[1]*Cátedra de Farmacognosia. Instituto de Farmacia. Facultad de Bioquímica, Química y Farmacia.*
Universidad Nacional de Tucumán. Ayacucho 471, 4000, San Miguel de Tucumán. Tucumán. Argentina.
[2]*Cátedra de Química General. Instituto de Química Inorgánica. Facultad de Bioquímica, Química y Farmacia.*
Universidad Nacional de Tucumán. Ayacucho 471, 4000, San Miguel de Tucumán. Tucumán. Argentina.
[3]*Cátedra de Química Orgánica. Facultad de Agronomía y Zootecnia, Universidad Nacional de Tucumán, Av. N. Kirchner*
1900, 4000, San Miguel de Tucumán, Argentina.

Abstract
Here, 2,8-dihydroxy-7H-furo[2,3-f]chromen-7-one (DHFC) has been isolated from *Tibouchina paratropica* medicinal plant and, then this species was experimentally characterized by using Fourier Transform infrared (FT-IR) and Hydrogen and Carbon Nuclear Magnetic Resonance (^{1}H- and ^{13}C-NMR) spectroscopies. The hybrid B3LYP/6-311++G** method was used to predict its structural, electronic, topological and vibrational properties in gas phase and in aqueous solution. Then, the complete vibrational assignments together with the harmonic force constants are reported. The studies by using the frontier orbitals support the higher reactivity of DHFC in solution, in agreement with the lower stability observed by NBO studies while the higher nucleophilic and electrophilicity indexes are observed in gas phase and in solution, respectively. The AIM study suggests that the furan ring is more dependent on electronic density than the other two rings. Better correlations between experimental FTIR and ^{1}H-NMR spectra with the corresponding predicted by the calculations were found.

1. Introduction

The structural and vibrational studies of 2,8-dihydroxy-7H-furo[2,3-f]chromen-7-one are interesting from a medical point of view because its phenolic derivative isolated from *Tibouchina paratropica* has evidenced antimicrobial activity towards some bacterial and fungal pathogens and, in addition, potent anti-parasitic activity against *Leishmania donovani* was also evidenced for this same compound [1].

So far, few references related to that interesting phenolic derivative were found in the literature and only some studies of triterpenes and flavonoids isolated from different varieties of genus *Tibouchina* (Melastomataceae) such as, semidecandra, pulchra, urvilleana, grandifolia, candolleana were reported [2-10]. Among these studies, the 2,6-dimethoxybenzoquinone derivative compound constituent of genus *Tibouchina Pulchra* is particularly interesting due to its anticancer properties [4].

In this work, the structural, electronic, topological and vibrational studies of 2,8-dihydroxy-7H-furo[2,3-f]chromen-7-one (DHFC) are carried out in gas phase and in aqueous solution in order to elucidate why this phenolic derivative shows those interesting biological activities. One of the purposes of this work is to examine the studies of structural properties of DHFC in the gas phase and in aqueous solution by combination of theoretical calculations derived from the density functional theory (DFT) with the hybrid B3LYP/6-311++G** method [11,12]. From natural bond orbital (NBO) and atoms in molecules (AIM) calculations, for DHFC in both media and at the same level of theory atomic charges, molecular electrostatic potentials, stabilization energies, bond orders and topological properties were predicted [13-15].

Currently, the structure of DHFC is not experimentally determined and, because of it, the optimized geometrical parameters were compared with those studied for the similar derivative 7,8-dihydroxy-2-H-chromen-2-one hemihydrate [16]. Another objective of this work is to determine the force fields of DHFC in both media by using the normal internal coordinates, transferable scale factors and the Scaled Quantum Mechanical Force Field (SQMFF) methodology together with the Molvib program [17-19]. After that, from the force fields, the complete vibrational assignments of DHFC in both media by comparisons between the predicted infrared spectra with the corresponding experimental recorded in the solid state are reported. Finally, calculations by using the frontier orbitals were also carry out for DHFC to predict reactivities and behaviour in both media taking into account the antimicrobial and anti-parasitic properties that that phenolic derivative presents[20-26]. Here, the properties obtained for DHFC in both media with those reported for other species containing similar OH, COO and C=O groups [27-33] were later compared.

2. Material and Methods
2.1. Extraction and isolation procedure
The extraction and isolation procedure of phenolic derivative, 2,8-dihydroxy-7H-furo[2,3-f]chromen-7-one (DHFC) was performed from the aerial parts of *Tibouchina paratropica*, as it is clearly carried out and explained in Ref [1].
2.2. Equipments
A pure sample of DHFC in the solid phase was prepared as KBr pellet in order to record the FTIR spectrum between 4000 to 400 cm^{-1} by using a Perkin Elmer GX spectrophotometer provided with a DTGS detector and constantly purged with dry air. In the registering of FTIR spectra a number of 256 scans and resolutions of 1 cm^{-} were used ^{1}.

Experimental ^{1}H- and 13C-NMR spectra of DHFC recorded in acetone-$_{d6}$ were already published and, for this reason, here, the observed chemical shifts were compared with the corresponding predicted in aqueous solution [1].
2.3. Computational details
The modelled of DHFC structure was carried out with the *GaussView* program [34] and then it was optimized in the gas phase and in aqueous solution at the B3LYP/6-311++G** level following the appropriate procedures [11,12,35,37] with the Gaussian 09 program [38]. The molecular structure of DHFC in **Figure 1** is given. Calculations of DHFC volume with the Moldraw program [39] and the study of electrostatic properties [40] in both media were performed. In addition, for this species bond orders, topological properties were computed using the NBO and AIM2000 programs [13-15], and with the gap values calculated from the border orbitals, reactivities, behaviour and some descriptors were predicted in both media [20-26]. The harmonic force fields of DHFC in both media were calculate by using the SQMFF procedure [17,18] and the Molvib program [19].
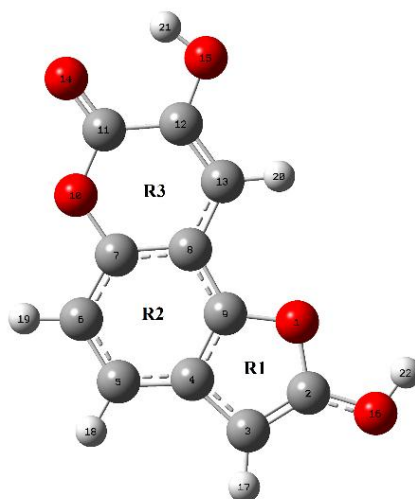

Figure 1: Molecular structure of 2,8-dihydroxy-7H-furo[2,3-f]chromen-7-one (DHFC) atoms numbering and identifications of three rings.

On the other hand, taking into account the corresponding force fields and potential energy distributions (PED), in the complete vibrational assignments of bands observed in the experimental infrared spectrum of DHFC in the solid phase were considered only those contributions ≥ 10%. Here, two dimeric species of DHFC which are shown in **Figure 2** are proposed due to the fact that some IR bands observed in the experimental spectrum which

are not assigned to the monomer can easily be justified by those two species. The predicted Raman spectrum intensities for DHFC, by using the same level of theory, were corrected using known equations [41,42]. The ^{1}H and ^{13}C chemical shifts of DHFC in aqueous solution were calculated by using the Gauge-Independent Atomic Orbital (GIAO) method [43] using to Trimethylsilane (TMS) as reference and, later, these values were compared with the corresponding experimental ones [1].
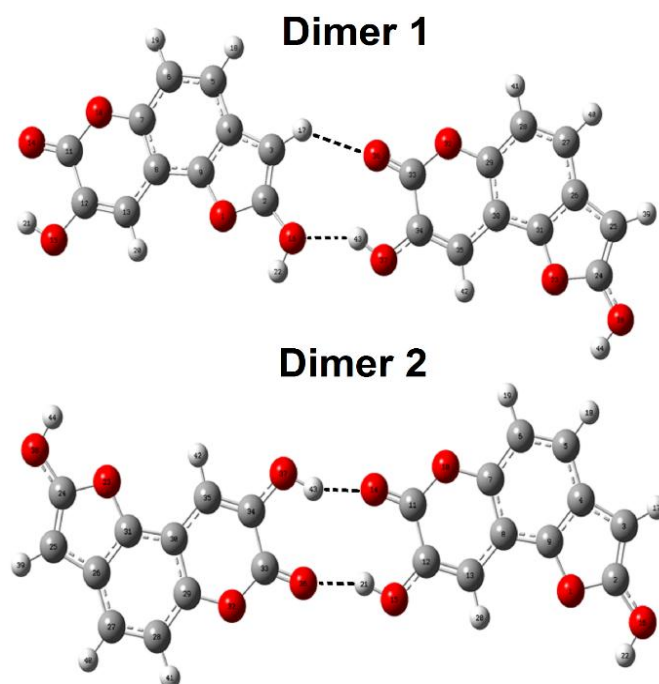

Figure 2: Molecular structures of two different dimeric species of 2,8-dihydroxy-7H-furo[2,3-f]chromen-7-one and atoms labelling

3. Results and discussion

3.1. Structural study in gas phase and in aqueous solution

Corrected total energies by zero point vibrational energy (ZPVE), dipole moments, volumes and volume variations calculated for DHFC in gas phase and in aqueous solution by using B3LYP/6-311++G** level of theory are presented in Table 1. Besides, corrected (ΔG_C) and uncorrected (ΔG_u) solvation energies by the total non-electrostatic terms (ΔG_{ne}) are shown in **Table 1**. The results reveal a higher increase of dipole moment value in solution and a slight expansion of volume in the same media. Despite this low increase of volume in solution, $\Delta V = 0.3$ Å^3, these changes can be easily attributed to the hydration of DHFC with water molecules. The orientations and directions of dipole moment vectors do not practically change in both media and only show clear variations in their magnitudes in solution, as it can be observed in **Figure S1**. In both cases, the directions of vectors are oriented towards the OH groups of furan rings. On the other side, the corrected solvation energy by the total non-electrostatic terms in water is -79.22 kJ/mol, a slightly higher value than that observed for the free base species of scopolamine alkaloid (-75.47 kJ/mol) and lower than the same species of heroin alkaloid (-88.67 kJ/mol) [44,45].

The calculated geometrical parameters for DHFC in both media were compared in **Table 2** with those experimentally observed for the similar derivative 7,8-dihydroxy-2-H-chromen-2-one hemihydrate [16] because, so far, its structure was not experimentally determined. In **Figure S2,** the common part of that structure with the corresponding to DHFC is shown in the red circle. The resulted of comparisons between theoretical and experimental parameters are quickly seen when the differences are presented by using the root-mean-square deviation (RMSD). Thus, reasonable correlations are observed in gas phase for bond lengths and angles (0.252 Å and 4.49º) while these correlations notably improve in solution with values of 0.082 Å for distances and 4.06 ° for angles. The differences observed in gas phase could be attributed to the different environments of the bonds C12-O15 and O15-H21 lengths and C12-O15-H21 angle in DHFC, as compared with the hemihydrate structure [16].

Table 1. Total Energy and moment dipolar for the 2,8-dihydroxy-7H-furo[2,3-f]chromen-7-one in gas phase and in aqueous solution by using the B3LYP/6-311++G** method. The corrected solvation energy of DHFC is also presented.

Property	Gas phase	Aqueous	ΔE(kJ/mol)	ΔV(Å^3)
		B3LYP/6-311++G**		
E (Hartrees)	-798.9681	-798.9871	-49.84	
μ(D)	3.79	5.92		
V(Å^3)	183.1	183.4		0.3

	Solvation energy (kJ/mol)		
Basis set	ΔG$_u$#	ΔG$_{ne}$	ΔG$_c$
6-311++G**	-49.84	29.38	-79.22

Z.P.V.E, zero point vibrational energy

Table 2. Comparison of calculated geometrical parameters for 2,8-dihydroxy-7H-furo[2,3-f]chromen-7-one in gas phase and in aqueous solution by using the B3LYP/6-311++G** method.

Parameters	Gas	PCM	Experimental [1]
	B3LYP/6-311++G**[a]		
	Bond lengths (Å)		
C4-C5	1.404	1.405	1.397
C5-C6	1.389	1.389	1.393
C6-C7	1.397	1.396	1.384
C7-C8	1.406	1.406	1.367
C8-C9	1.395	1.396	1.400
C9-C4	0.398	1.398	1.380
C8-C13	1.436	1.433	1.435
C7-O10	1.379	1.387	1.490
C11-O10	1.356	1.358	1.339
C11-C12	1.470	1.458	1.442
C12-C13	1.351	1.353	1.340
C12-O15	1.348	1.361	1.336
C11=O14	1.212	1.223	1.224
O15-H21	0.972	0.971	0.795
C5-H18	1.083	1.083	0.931
C6-H19	1.083	1.083	0.931
C13-H20	1.083	1.083	0.930
RMSD	**0.252**	**0.082**	
	Bond angles (º)		
C5-C4-C9	118.6	118.8	120.0
C4-C5-C6	118.9	119.0	121.6
C5-C6-C7	120.3	119.9	115.0
C6-C7-C8	123.1	123.6	126.9
C7-C8-C9	114.3	114.2	116.6
C7-O10-C11	122.6	122.8	119.2
O10-C11-C12	117.5	117.7	120.0
C11-C12-C13	121.5	121.3	111.1
C12-C13-C8	118.9	119.3	120.7
C7-C8-C13	119.6	119.6	119.3
O10-C11-O14	120.5	118.9	113.3
C12-C11-O14	122.0	123.4	126.6
C12-O15-H21	106.7	108.2	108.2

RMSD[a]	**4.49**	**4.06**	
Diedral angles (°)			
C9-C8-C7-O10	180.0	180.0	179.3
C7-O10-C11-O14	180.0	180.0	177.6
RMSD[b]	**1.77**	**1.77**	

[a]This work, [b]From Ref. [17]

From Table 2, we observed that some parameters are predicted with higher values than the experimental ones while the C11=O14 and C12=C13 bonds are predicted with double bonds characters. In relation to the angles, the higher RMSD values are observed in the bond angles (4.49-4.06 °) as compared to the dihedral ones, a different result than those observed for other molecules [27,28,44,45]. Here, two dimeric species for DHFC are also proposed according to the intra-molecular O-H---O hydrogen bonds observed in the molecular packing determined for the experimental crystalline structure of 7,8-dihydroxy-2-H-chromen-2-one hemihydrate [16]. The graphic of molecular structures of both dimers in **Figure 2** are given. Therefore, it is expected that the H bonds stabilize the molecular conformation of DHFC due to the presence of C=O and OH bonds, as reported for that hemihydrate [16].

3.2. Charges, bond orders and molecular electrostatic potentials studies

The atomic natural population (NPA) and Merz-Kollman (MK) charges are important parameters that describe the different hydrophilic and hydrophobic sites and, consequently they could possibly explain the biological properties evidenced for DHFC in both media [1-5]. Hence, for this phenolic derivative in the two media both calculated charges by using the B3LYP/6-311++G** method are summarized in **Table S1** while the behaviours of MK and NPA charges with the different media are shown in **Figure S3**. From Figure S3, first we observed that, the values of MK charges in both media practically do not change (light blue and brown lines) and only a less positive value in the MK charge on C4 atom in gas phase is observed while its atom in solution has a high value. On the contrary, the NPA charges generally show a substantial difference in solution. Thus, these NPA charges on the C4 and C6 atoms present the most negative values while the most positive charges can be seen on the C8 and C11 atoms. Another very important result is the most negative NPA charges observed on all O atoms in solution, in particular on the O16 atom while the MK charges on these atoms present lower values. In reference to the H atoms, the NPA charges on the H21 and H22 atoms of both OH groups present the most positive values, as it was expected because strong electrophilic sites are expected on these atoms. The evaluation of the NPA charges on O atoms, in both media, shows strong nucleophilic regions on the O16 atoms.

The characteristics of the different bonds that present DHFC in both media were studied through of bond orders (BO), expressed as Wiberg indexes, and they are computed with the NBO program [13] by using the B3LYP/6-311++G** method. The resulted for DHFC in both media are given in **Table S2** while their variations in the two media can be seen in **Figure S4**. The behaviours of BOs in both media are practically the same for all atoms with exception of C4, C5, C6, C8 and H18 atoms whose values change notably in solution, presenting higher variations in this medium the C4, C8 and H18 atoms. These variations in solution quickly show that the bonds characters where the three atoms are involved change with the medium. Thus, the BO corresponding to the atoms involved in the C11=O14 bond decrease in solution, a behaviour similar to the one observed in the H21 and H22 atoms, probably due to the hydration of these bonds with water molecules. Hence, the double bond character of C11=O14 bond slightly decreases in solution.

The mapped electrostatic potentials (MEP) surfaces are useful to find those specific different nucleophilic, electrophilic, and inert sites reaction sites by using the different colours. Thus, these surfaces are of particular interest in DHFC due to the presence of O atoms and of C=O and OH groups with different hydrophobic and hydrophilic characteristics. Hence, the molecular electrostatic potentials values computed on all atoms of DHFC by using the atomic Merz-Kollman (MK) charges [40] do not present significant differences in both media and, for these reasons, they were not presented here. However, the observed tendency is O > C > H, as it was expected due to its different electronegativities. Nevertheless, the mapped MEP surface for DHFC in gas phase was performed by using the B3LYP/6-311G** method because the generation of mapped MEP surface was not possible with the basis set of higher size. Here, the mapped MEP surface for DHFC in gas phase is shown in **Figure S5**. This figure shows a strong red colour on the C11=O14 group while on the H21 and H22 atoms of two OH groups blue colours are observed. Hence, on the C11=O14 group the nucleophilic site is clearly shown while the electrophilic sites are evidenced on the H atoms of both OH groups. Evidently, the green colours on both benzene rings simply indicate inert regions.

3.3. NBO and AIM studies

In order to explain the pharmacological properties, DHFC, NBO and AIM calculations [13-15] were carried out for this phenolic derivative in gas phase and in aqueous solution by using different sizes of basis set. Hence, the donor-acceptor energy interactions computed at the B3LYP/6-311G** level of theory are presented with the NBO program [13] in **Table S3**, while their topological properties calculated in the ring critical point (RCP) with the AIM2000 program in both media by using the B3LYP/6-311++G** method [15] are summarized in **Table S4**. Here, it is necessary to explain that when the 6-311++G** basis set is employed, interactions were not observed; however, when the diffuse functions were removed from the calculations, five different interactions type appear in Table S3 in both media. Thus, the interaction observed by using the B3LYP/6-311G** level of theory are $\Delta ET_{\pi \to \pi*}$, $\Delta ET_{LP \to \sigma*}$, $\Delta ET_{LP \to \pi*}$, $\Delta ET_{\sigma* \to \sigma*}$ and $\Delta ET_{\pi* \to \pi*}$, while the latter interaction is the most energetic. The resultant total energy slightly favours DHFC in gas phase 3109.96 kJ/mol, in reference to its value in solution of 3093.76 kJ/mol. This result clearly indicates that the species in solution is less stable and, for this reason, it presents a higher reactivity in this medium, as we will see later by using the frontier orbitals studies.

The Bader's theory is useful to predict different intra-molecular, inter-molecular, ionic or of H bonds interactions [14] knowing the topological properties calculated in the bond critical points (BCPs) or ring critical points (RCPs). Thus, the electron density distribution, $\rho(r)$, the values of the Laplacian, $\nabla^2\rho(r)$, the eigenvalues ($\lambda1$, $\lambda2$, $\lambda3$) of the Hessian matrix and the $\lambda1/\lambda3$ ratio for DHFC in the two media are presented in Table S4. The results do not show new BCPs and only RCPs are observed. **Figure 3** shows the three RCPs corresponding to the three own rings of DHFC calculated with the AIM2000 program in both media and by using the B3LYP/6-311++G** method [15]. Note that the RCP1 corresponding to furan ring shows higher topological properties while the RCP3 shows lower values. In solution, the properties of RCPs notably change showing a decrease in the electron density of RCP1 whiles the Laplacian values increase in the three rings. These studies clearly show that the furan ring (RCP1) is the most dependent of medium through of $\rho(r)$, however, RCP3 is less influenced by the medium.

3.4. Frontier orbitals and descriptors studies

The NBO analysis has evidenced five different transitions for DHFC while the AIM studies support the different characteristics of three rings of this phenolic derivative, presenting the R1 ring, the furan ring, higher topological properties in both studied media. Thus, it is necessary to investigate the reactivities and behaviours of DHFC in the two media. Hence, from the differences between the frontiers orbitals its gap values were predicted, as recommended by Parr and Pearson [20]. Later, the chemical potential (μ), electronegativity (χ), global hardness (η), global softness (S) and global electrophilicity index (ω) descriptors were calculated with the gap values by using the suggested equations [32-41] and, the results are presented in **Table S5.** These results show higher reactivity of DHFC in solution, in agreement with the NBO studies while higher nucleophilic and electrophilicity indexes are observed in gas phase and in solution, respectively. Probably, the increase of electrophilicity index in solution is associated to an increase of values of the Laplacian in the three rings in solution while the diminishing of electron density of RCP1 in this medium could in part justify the decrease of nucleophilicity index in solution. Probably, the O atom and the OH group belong of furan ring should be hydrated in solution.
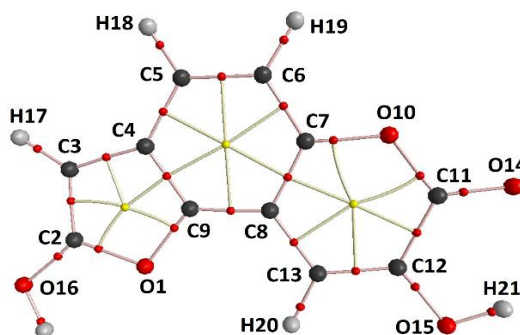

Figure 3: Molecular graphics for 2,8-dihydroxy-7H-furo[2,3-f]chromen-7-one in gas phase showing the geometry of all their bond critical points (BCPs) and ring critical points (RCPs) at the B3LYP/6-311++G** level of theory.

3.5. Vibrational analysis

The DHFC structures in both media were optimized with C_1 symmetries by using the B3LYP/6-311++G** method for which the expected 60 vibration normal modes present activities in both infrared and Raman spectra. The experimental IR spectrum of DHFC in the solid state compared with the corresponding predicted in the two media are given in **Figure 4** while the predicted Raman spectra of DHFC in both media are compared in **Figure 5**. For a better correlation, the predicted Raman spectra in activities were transformed to intensities applying

classical suggested equations from the literature [41,43]. The intense and broad IR bands observed in the experimental spectrum in the 4000-2000 cm^{-1} region clearly indicate the presence of O-H---O bonds belonging to dimeric species of DHFC in the solid phase due to crystal packing, as was observed in the experimental crystalline structure of 7,8-dihydroxy-2-H-chromen-2-one hemihydrate [16].
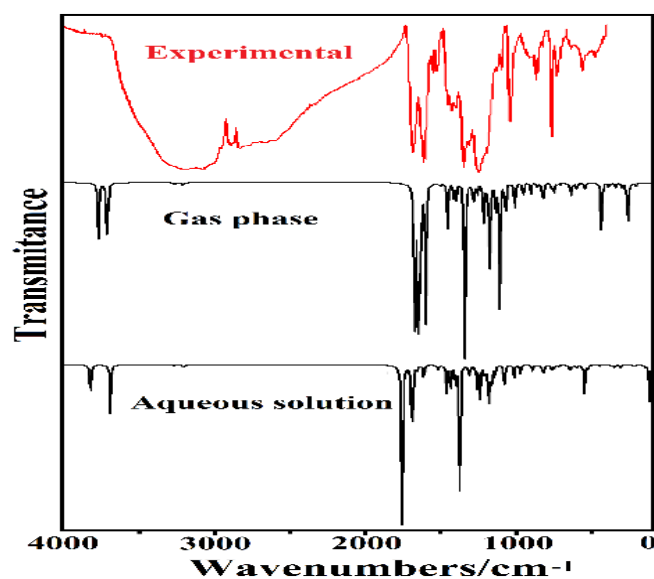

Figure 4: Experimental infrared spectra of 2,8-dihydroxy-7H-furo[2,3-f]chromen-7-one (upper) in the solid state compared with the corresponding predicted in gas phase (medium) and in aqueous solution (bottom) by using the B3LYP/6-311++G** level of theory.
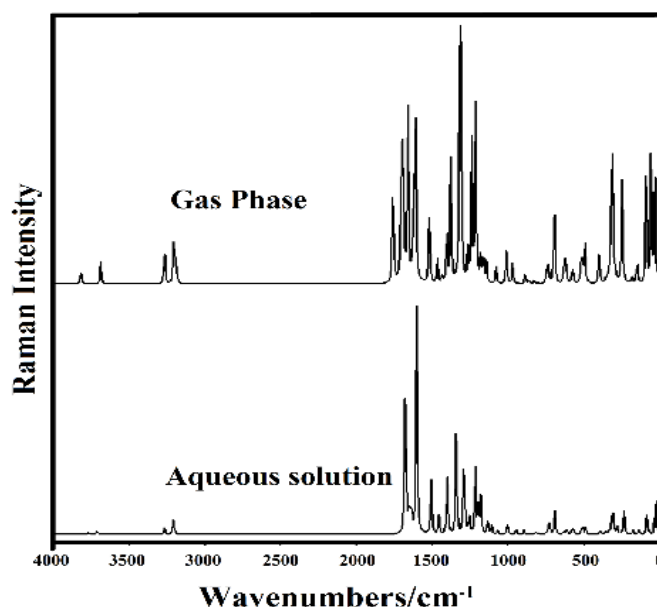

Figure 5: Predicted Raman spectra of 2,8-dihydroxy-7H-furo[2,3-f]chromen-7-one in gas phase and in aqueous solution by using the B3LYP/6-311++G** level of theory.

Hence, the comparisons between the predicted IR spectra for the two dimers with that experimental recorded for DHFC in the solid state is shown in **Figure S6**. This latter figure shows clearly that the very intense IR band of dimer 2 at 3558 cm^{-1} region clearly justify the intense and wide band observed in the experimental spectrum in the higher wavenumbers region. Hence, the strong and broad band centred in 3206 cm^{-1} is easily attributed to the OH stretching modes while the bands between 3000 and 2500 cm^{-1} are associated to H bonds of dimeric species. The presence of impurity of sample or to combination bands could be associated to the strong IR band at 2830 cm^{-1}, as is detailed in Table 3. The harmonic force fields of DHFC in both media by using the B3LYP/6-311++G** level of theory were calculated with the SQMFF procedure and the Molvib program taking into account the normal internal coordinates and useful scale factors [17-19]. Later, the complete vibrational

assignments of bands observed in the experimental IR spectrum of DHFC in both media is carried out with the harmonic force fields and considering potential energy distribution (PED) contributions $\geq 10\%$. On the other hand, the observed and calculated wavenumbers and assignments for DHFC in the gas phase and in aqueous solution are presented in **Table 3**. Below, we present a brief discussion of main vibration modes.

Table 3. Observed and calculated wavenumbers (cm^{-1}) and assignments for 2,8-dihydroxy-7H-furo[2,3-f]chromen-7-one in gas phase and in aqueous solution by using the B3LYP/6-311++G** method.

Experimental	GAS			PCM		
	Calculated	SQM	Asignación	Calculated	SQM	Asignación
3206 br,s	3819	3661	νO16-H22	3765	3609	νO16-H22
3206 br,s	3687	3535	νO15-H21	3709	3555	νO16-H22
3073 s	3267	3131	νC3-H17	3264	3129	νC3-H17
2996 s	3206	3073	νC6-H19	3209	3076	νC6-H19
2947 s	3202	3069	νC13-H20	3206	3073	νC13-H20
2947 s	3189	3057	νC5-H18	3196	3064	νC5-H18
2830 s	2x765=1530 + 1311 = 2841					
1682 s	1757	1692	νC11=O14	1680	1620	νC13=C12
1682 s	1697	1637	νC13=C12	1672	1614	νC11=O14
1682 s	1691	1628	νC2=C3	1652	1590	νC2=C3
1607 s	1658	1604	νC4=C9	1636	1579	νC8-C9
1550 w	1613	1561	νC4=C5	1602	1549	νC4=C5
1528 w	βC-H dimer 2					
1456 m	1517	1467	νC5-C6	1506	1456	νC7-C8
1426 m	1465	1418	βC5-H18	1457	1410	νC4=C9
1395 m	1435	1385	δO15-H21			
1376 sh	δO-H dimer 2			1416	1370	νC6-C7
1345 s	1403	1353	νC8-C9	1400	1351	νC5-C6
1311 s	1376	1329	νC2-O16	1343	1301	νC3-C4
1241 vs	1316	1271	νC8-C13	1293	1246	νC9-O1
1241 vs	1308	1261	νC3-C4	1283	1238	δO16-H22
1241 vs	1264	1222	νC6-C7	1258	1221	νC8-C13
1194 sh	1241	1193	βC13-H20	1218	1161	δO15-H21
1194 sh	1215	1173	νC7-O10; νC12-O15			
1194 sh	1204	1162	βC3-H17	1198	1153	βC13-H20
1134 w	1182	1142	βC6-H19	1184	1145	νC2-O16
1123 sh	1164	1123	νC11-O10	1175	1135	βC5-H18
1097 w	1143	1103	δO16-H22	1138	1101	βC3-H17
1041 s	1081	1048	νC9-O1	1113	1077	νC11-O10
1041 s	βR1(A2) Dimer 2			1074	1041	βC6-H19
959 w	1014	984	νC7-C8	1011	980	νC7-O10
941 w	975	944	νC2-O1	955	945	γC5-H18
941 w	946	936	γC6-H19	954	926	νC2-O1
905 br	894	884	γC13-H20	904	895	γC13-H20
865 m	869	851	βR1 (A2)	864	849	βR1 (A2)
821 w	838	817	βR1 (A3)			
788 vw	820	808	γC5-H18	832	808	γC6-H19
765 s	γC-H dimer 2			820	808	νC12-O15
765 s	767	759	γC3-H17	765	756	γC3-H17

	756	740	γC11-O14	752	743	γC11-O14
734 m	749	739	βR1 (A1)	747	729	βR1 (A1)
720 m	720	700	νC12-C11	727	705	τR1 (A2)
720 m	714	699	τR1 (A2)	711	698	βR1 (A3) νC12-C11
662 sh	657	642	γC2-O16	659	644	γC2-O16
640 w	645	638	βR2 (A2)	642	635	βR2 (A2)
	627	609	τR3 (A2)	630	611	τR3 (A2)
602 sh	603	595	βR2 (A3)	604	596	βR2 (A3)
561 w	552	544	τO15-H21	547	543	βR3 (A2)
561 w	547	542	βC2-O16			
474 w	530	521	βR2 (A1)	531	518	βR2 (A1)
449 w	527	512	τR2 (A2)	527	515	τR2 (A2)
442 w	446	440	βR3 (A3)	445	438	βR3 (A3)
432 w	γC-O Dimer 2			439	433	τO15-H21
413 w	405	400	γC12-O15	409	404	γC12-O15
	388	377	Butt (A2-A3)	390	379	Butt (A2-A3)
	371	364	βR3 (A2)	372	365	βC2-O16
	354	345	τR2 (A1)	357	348	τR2 (A1)
	350	345	βC11-O14	344	339	βC11-O14
	313	310	βC12-O15	303	301	βC12-O15
	τR1(A3) dimer 2			266	253	τO16-H22
	252	244	τR1(A3)	249	240	τR1 (A3)
	220	213	τR1 (A1)	212	203	τR1 (A1)
	157	154	βR3 (A2); βR3 (A3)	157	155	βR3 (A2); βR3 (A3)
	144	140	Butt (A1-A2)	137	133	βR3 (A2)
	120	120	τO16-H22			
	96	94	τR2 (A3)	94	91	τR2 (A3)
	74	71	τR3 (A3)	68	66	τR3 (A3)

Abbreviations: ν, stretching; β, deformation in the plane; γ, deformation out of plane; τ , torsion; $β_R$, deformation ring $τ_R$, torsion ring; δ, deformation; (A1), Ring 1; (A2), Ring 2; (A3), Ring 3; [a]This work, [b]From scaled quantum mechanics force field, br, broad; s, strong; w, weak;m, medium; vs, very strong; vw, very weak

3.5.1. Band Assignments

3.5.1.1. OH modes. Two O15-H21 and O16-H22 groups are present in the DHFC structure that belong to R3 and R1 rings, respectively. Hence, for this phenolic derivative two OH stretching modes are expected. Thus, the broad and intense IR band at 3206 cm^{-1} region is quickly assigned to those two vibration modes, as observed in species containing these groups [22,24-33,44,45]. The SQM calculations predicted the in-plane deformation modes of those two OH groups in gas phase at 1385 and 1103 cm^{-1} while in aqueous solution at 1238 and 1161 cm^{-1}, hence, the IR band at 1395, 1241, 1194 and 1097 cm^{-1} are assigned to these modes. The out-of-plane deformation or torsion modes expected for those two OH groups are predict by SQM calculations at 544, 433, 253 and 120 cm^{-1} and, for these reasons, the bands at 561 and 432 cm^{-1} are assigned to those modes. The assignments of other modes were not possible due to the absence of IR bands in the lower wavenumbers region, as observed in Table 3.

3.5.1.2. CH modes. In the higher wavenumbers region four C-H stretching modes are present in DHFC because it has the C3-H17 group that belongs to the furan ring, the C13-H20 group that belongs to the R3 and the two remaining groups that belong to the R2 ring. Hence, the SQM calculations predict these stretching modes between 3131 and 3057 cm^{-1}, while those stretching modes are predicted in both media at higher wavenumbers than the other ones. Thus, the IR bands between 3073 and 2947 cm^{-1} can easily be assigned to those vibration modes. Here, it is interesting to note that the SQM calculations predict the C3-H17 stretching modes at higher wavenumbers in both media than the other ones. The in-plane deformations or rocking modes corresponding to the four C-H groups

in both media are predicted between 1418 and 1041 cm^{-1}, for which, they are associated to the groups of IR bands between 1426 and 1041 cm^{-1}. The IR bands from 941 up to 756 cm^{-1} are assigned to out-of-plane deformations or wagging modes of C-H bonds, as predicted by SQM calculations.

3.5.1.3. Skeletal modes. Usually, the C=O stretching modes are assigned between 1741 and 1636 cm^{-1} [22,24-33], hence, the very strong IR band at 1682 cm^{-1} is clearly assigned to those two stretching modes. Note that this stretching mode is predicted shifted from 1692 cm^{-1} in gas phase to 1614 cm^{-1} in aqueous solution due to the hydration of C=O group with water molecules. Here, the strong IR band at 1682 cm^{-1} can also be assigned to C=C stretching modes because these vibration modes are predicted between 1637 and 1549 cm^{-1}. Other C-C and C-O stretching modes can be assigned between 1456 and 720 cm^{-1}, as observed in Table 3 [24-33,44,45]. For instance, these C-O stretching modes in carquejol [28] are predicted between 1063 and 1020 cm^{-1} and assigned at 1065 cm^{-1}. In DHFC, a slight shifting of the two C-O stretching modes related to C-OH groups in solution is observed, in relation to the values in gas phase, due to the hydration of these groups with water molecules. We assigned the deformation and torsion modes corresponding to six and five member rings as the theoretical calculations predicted and, as it was reported in similar molecules [22-33,44,45]. The assignments of remain skeletal modes are clearly detailed in Table 3.

4. Force Fields

The harmonic force fields by using the B3LYP/6-311++G** method were calculated by using the SQMFF methodology in order to compute the scaled force constants for DHFC in the gas phase and in aqueous solution [17,18] and the Molvib program [19]. In **Table 4,** these constants are compared with the reported for 2R-(−)-6-hydroxytremetone in gas phase [33].

Table 4. Comparison of main scaled internal force constants for 2,8-dihydroxy-7H-furo[2,3-f]chromen-7-one in gas and aqueous solution phases with those reported for 2R-(−)-6-hydroxytremetone in gas phase.

Force constants	B3LYP/6-311++G**[a]		B3LYP/6-31G**	
			2R-(−)-6-hydroxytremetone[b]	
	Gas	PCM	A	B
$f(\nu O\text{-}H)$	7.242	7.180	5.256	5.252
$f(\nu C\text{-}O)$	6.406	5.586	6.858	6.861
$f(\nu C\text{-}H)_{A6}$	5.167	5.176	6.522	6.526
$f(\nu C\text{-}H)_{A6bis}$	5.152	5.164		
$f(\nu C\text{-}H)_{A5}$	5.375	5.344	4.758	4.613
$f(\nu C\text{-}C)_{A6}$	6.211	6.221	6.520	6.526
$f(\nu C\text{-}C)_{A5}$	6.423	6.410	3.988	3.982
$f(\nu C\text{=}O)$	11.506	10.303	10.248	10.249
$f(\nu C\text{-}O)_{A6}$	5.133	4.852		
$f(\nu C\text{-}O)_{A5}$	5.162	4.873	4.852	4.976
$f(\delta O\text{-}H)$	0.737	0.721	1.113	1.131
$f\beta_R (A_5)$	0.368	0.366		
$f\beta_R (A_6)$	0.248	0.247		
Butt	2.527	2.469		

Units are mdyn Å^{-1} for stretching and mdyn Å rad^{-2} for angle deformations [a]This work; [b]From Ref [34]

Evaluating first the force constants for DHFC in the two media, we observed that the values of $f(\nu O\text{-}H)$, $f(\nu C\text{=}O)$ and $f(\nu C\text{-}O)$ force constants in aqueous solution present lower values than the corresponding in gas phase probably because the related groups are hydrated with solvent molecules. The other force constants practically present the same values in both media. If now the values observed for DHFC are compared with the corresponding to 2R-(−)-6-hydroxytremetone lower values are observed in the $f(\nu O\text{-}H)$ force constants of 2R-(−)-6-hydroxytremetone. In part, such differences could be attributed to the presence of only a OH group in the other species while in DHFC there are two OH groups or, also could be associated to the formation of H bonds where these groups are involved in 2R-(−)-6-hydroxytremetone. Hence, the hydration of these groups could also justify the lower values observed in the $f(\delta O\text{-}H)$ force constants of DHFC, as compared with the observed for 2R-(−)-6-hydroxytremetone [33].

5. NMR study

In this work, the ^{1}H- and ^{13}C-NMR chemical shifts of DHFC predicted in aqueous solution by using the GIAO method [44] with the hybrid B3LYP/6-311++G** method are compared the corresponding taken from those experimental ^{1}H- and ^{13}C-NMR spectra previously recorded in acetone-$_{d6}$ [1]. The results of both comparisons by means of the RMSD values can be seen in **Tables 5** and **6**.

In general, we observed that the predicted values are overestimated as compared with the experimental ones and a better concordance it is observed for the ^{1}H nucleus (1.02-0.97 ppm) while for the ^{13}C nucleus the correlation is not very good and the RMSD values are high (27.65-23.26 ppm), as was also observed for carquejol [28]. Here, the chemical shifts for both H21 and H22 nucleus are not predicted probably because both atoms in solution are involved in the hydrogen bonding formation with solvent molecules. As it is expected, better correlations are obtained for the ^{1}H nucleus than the C atoms because the used 6-311++G** basis set favours to the light atoms than the C ones.

Table 5. Observed and calculated ^{1}H chemical shifts (δ in ppm) for 2,8-dihydroxy-7H-furo[2,3-f]chromen-7-one in different media by using the B3LYP/6-311++G** method

H Atoms	^{1}H-NMR[a]			
	6-311++G**		Experimental in acetone-d6[b]	
	Gas	PCM	δ ppm	Integ. Multiplicity (JHz)
22	4.60	5.56		
21	6.02	5.77		
17	5.46	5.74	7.42	1H s
20	7.20	7.71	7.04	1H br s
18	7.29	7.54	7.40	1H d (8.8)
19	7.32	7.45	6.78	1H d (8.8)
RMSD	**1.02**	**0.97**		

[a]This work GIAO/B3LYP/6-311++G** Ref. to TMS, [b]From Ref [1]

Table 6. Observed and calculated ^{13}C chemical shifts (δ in ppm) for 2,8-dihydroxy-7H-furo[2,3-f]chromen-7-one in different media by using the B3LYP/6-311++G** method

C Atoms	^{13}C-NMR[a]		
	6-311++G**		Experimental in acetone-d6[b]
	Gas	PCM	δ ppm
C3	97.46	80.63	116.6
C13	126.77	114.87	109.3
C8	128.86	111.64	145.0
C6	134.95	116.78	114.7
C5	139.47	124.20	122.8
C4	150.44	133.98	150.1
C12	164.89	146.05	120.8
C9	165.20	148.84	138.3
C7	169.73	153.01	168.7
C11	180.79	165.86	168.9
C2	184.99	169.28	121.9
RMSD	**27.65**	**23.26**	

[a]This work GIAO/B3LYP/6-31G* Ref. to TMS, [b]From Ref [1]

Conclusions

In the present work, the phenolic 2,8-dihydroxy-7H-furo[2,3-f]chromen-7-one (DHFC) derivative has been isolated from *Tibouchina paratropica* medicinal plant and later it was characterized by using FTIR and ^{1}H- and ^{13}C-NMR spectroscopies. Here, hybrid B3LYP/6-311++G** calculations were employed in order to study their structural, electronic, topological and vibrational properties in gas phase and in aqueous solution. For DHFC, two dimeric species were proposed taking into account the experimental structure of similar derivative 7,8-dihydroxy-2-H-chromen-2-one hemihydrate because, so far, its structure was not reported. Thus, O-H---O hydrogen bonds interactions of those two dimeric species could stabilize the molecular conformation, as supported by the intensities and forms of some bands observed in the experimental IR spectrum. The SQMFF methodology at the same level of theory was used to calculate the harmonic force fields for DHFC in the two media. Then, the complete vibrational assignments of expected 60 vibration modes together with the harmonic force constants are here reported for first time. The molecular electrostatic potentials (MEP) surface suggest that the nucleophilic site is clearly located on the C=O group while the electrophilic sites are located on the H atoms of both OH groups. The studies by using the frontier orbitals support higher reactivity of DHFC in solution, in agreement with the lower stability observed by NBO studies while the higher nucleophilic and electrophilicity indexes are observed in gas phase and in solution, respectively. The AIM study shows clearly that the furan ring (RCP1) is most dependent of medium through of $\rho(r)$ than the other rings. Better correlations between experimental FTIR and ^{1}H-NMR spectra with the corresponding predicted by the calculations were found.

Supporting Information Available: Tables S1-S5 and **Figures S1-S6**.

References

1. M.I. Tracanna, A.M. Fortuna, A.V. Contreras Cárdenas, A.K. Marr, W.R. McMaster, A. Gómez-Velasco, E. Sánchez-Arreola, L.R. Hernández, H. Bach, Anti-leishmanial, anti-inflammatory and antimicrobial activities of phenolic derivatives from *Tibouchina paratropica*, Phytother Res. 29(3) (2015) 393-397. https://doi.org/10.1002/ptr.5263
2. P. Peralta, Las especies del género *Tibouchina* (Melastomataceae) en Argentina, Darwiniana. 40 (1-4) (2002) 107-120.
3. T. Yoshida, W. Ohwashi, K. Haba, H. Ohbayashi, K. Ishihara, Y. Okano, T. Shingu, T. Okuda, Tannins and related polyphenols of Melastomataceous Plants. II.[1)] Nobotanins B, C and E, hydrolyzable tannin dimer and trimers from *Tibouchina Semidecandra* COGN, Chem. Pharm. Bull. 39 (9) (1991) 2264-2270. https://doi.org/10.1248/cpb.39.2264
4. E. Jones, O. Ekundayo, D.G.I. Kinston, Plant anticancer agents. XI. 2,6-Dimethoxybenzoquinone as a cytotoxic constituent of *Tibouchina Pulchra*, J. Nat. Prod. 44 (4) (1980) 493-494. https://doi.org/10.1021/np50016a019
5. H. M. Sirat, M. F. Rezali, Z. Ujang, Isolation and identification of radical scavenging and tyrosinase inhibition of polyphenols from *Tibouchina semidecandra* L, J. Agric. Food Chem. 58 (2010) 10404–10409. https://doi.org/10.1021/jf102231h
6. A.L. Pérez- Castorena, Triterpenes and other metabolites from *Tibouchina urvilleana*, *J. Mex. Chem. Soc.* 58 (2) (2014) 218-222.
7. R. M. Kuster, N. Arnold, L. Wessjohann, Anti-fungal flavonoids from *Tibouchina grandifolia*, Biochem. Syst. .Ecol. 37 (2009) 63-65.
8. F.M. dos Santos, M. G.de Souza, A.E. Miller Crotti, C. H. G. Martins, S. R. Ambrósio, R.C.S. Veneziani, M.L. Andrade e Silva, W.R. Cunha, Evaluation of antimicrobial activity of extracts of *Tibouchina Candolleana* (Melastomataceae), isolated compounds and semi-synthetic derivatives against endodontic bacteria, Braz. J. Microbiol. 43 (2012) 793-799. http://dx.doi.org/10.1590/S1517-83822012000200045
9. J.H. Isaza M, A. García Vivas, A. Londoño M, F.J. Jiménez G, J.C. Sepúlveda, L.A. Veloza C, L.S. Ramirez A, Determinación espectrofotométrica de la actividad inhibitoria de xantina oxidasa en extractos de algunas plantas Melastomataceas, Scientia et Technica Año XIII, (33) (2007) 307-310.

10. A.V. de Mello Cruz, M.A. Coelho Kaplan, Uso medicinal de espécies das famílias Myrtaceae e Melastomataceae no Brasil, Floresta e Ambiente, 11 (1) (2004) 47-52.

11. A.D. Becke, Density-functional exchange-energy approximation with correct asymptotic behavior, Phys. Rev. A38 (1988) 3098-3100.

12. C. Lee, W. Yang, R.G. Parr. Development of the Colle-Salvetti correlation-energy formula into a functional of the electron density, Phys. Rev. B37 (1988) 785-789.

13. E.D. Glendening, J.K. Badenhoop, A.D. Reed, J.E. Carpenter, F. Weinhold, NBO 3.1; Theoretical Chemistry Institute, University of Wisconsin; Madison, WI, 1996.

14. R.F.W. Bader, Atoms in Molecules, A Quantum Theory, Oxford University Press, Oxford, 1990, ISBN: 0198558651.

15. F. Biegler-Köning, J. Schönbohm, D. Bayles, AIM2000; A Program to Analyze and Visualize Atoms in Molecules, J. Comput. Chem. 22 (2001) 545.

16. Y.B Lu, Q.T. Zheng, Y. Lu, Redetermination of 7,8-dihydroxy-2-H-chromen-2-one hemihydrate, Acta Cryst. E62 (2006) o5315-o5316. https://doi.org/10.1107/S1600536806036919

17. P. Pulay, G. Fogarasi, G. Pongor, J.E. Boggs, A.Vargha, Combination of theoretical ab initio and experimental information to obtain reliable harmonic force constants. Scaled quantum mechanical (QM) force fields for glyoxal, acrolein, butadiene, formaldehyde, and ethylene, J. Am. Chem. Soc. 105 (1983) 7037-7047. https://doi.org/10.1021/ja00362a005 .

18. a) G. Rauhut, P. Pulay, Transferable Scaling Factors for Density Functional Derived Vibrational Force Fields, J. Phys. Chem. 99 (1995) 3093-3100; https://doi.org/10.1021/j100010a019 .
b) G. Rauhut, P. Pulay, J. Phys. Chem. 99 (1995) 14572.

19. T. Sundius, Scaling of ab-initio force fields by MOLVIB, Vib. Spectrosc. 29 (2002) 89-95. https://doi.org/10.1016/S0924-2031(01)00189-8.

20. R.G. Parr, R.G. Pearson, Absolute hardness: companion parameter to absolute electronegativity, J. Am. Chem. Soc. 105 (1983) 7512-7516. https://doi.org/10.1021/ja00364a005.

21. J-L Brédas, Mind the gap!, Mater. Horiz. 1 (2014) 17–19. DOI: 10.1039/C3MH00098B

22. D. Romani, S.A. Brandán, M.J. Márquez, M.B. Márquez, Structural, topological and vibrational properties of an isothiazole derivatives series with antiviral activities, J. Mol. Struct. 1100 (2015) 279-289. https://doi.org/10.1016/j.molstruc.2015.07.038.

23. D. Romani, S. Tsuchiya, M. Yotsu-Yamashita, S.A. Brandán, Spectroscopic and structural investigation on intermediates species structurally associated to the tricyclic bisguanidine compound and to the toxic agent, saxitoxin, J. Mol. Struct. 1119 (2016) 25-38. https://doi.org/10.1016/j.molstruc.2016.04.039.

24. E. Romano, M.V. Castillo, J.L. Pergomet, J. Zinczuk, S.A. Brandán, Synthesis, structural and vibrational analysis of (5,7-Dichloro-quinolin-8-yloxy) acetic acid, J. Mol. Struct. 1018 (2012) 149–155. https://doi.org/10.1016/j.molstruc.2012.03.013.

25. M.A. Iramain, L. Davies, S.A. Brandán, Structural and spectroscopic differences among the Potassium 5-hydroxypentanoyltrifluoroborate salt and the furoyl and isonicotinoyl salts, J Mol. Struct. 1176 (2019) 718-728. https://doi.org/10.1016/j.molstruc.2018.09.015.

26. N. Issaoui, H. Ghalla, S.A. Brandán, F. Bardak, H.T. Flakus, A. Atac, B. Oujia, Experimental FTIR and FT-Raman and theoretical studies on the molecular structures of monomer and dimer of 3-thiopheneacrylic acid, J. Mol. Struct. 1135 (2017) 209-221. https://doi.org/10.1016/j.molstruc.2017.01.074

27. M. Minteguiaga, E. Dellacassa, M.A. Iramain, C.A.N. Catalán, S.A. Brandán, FT-IR, FT-Raman, UV-Vis, NMR and structural studies of carquejyl acetate, a distinctive component of the essential oil from Baccharis trimera (Less.) DC. (Asteraceae), J Mol. Struct. 1177 (2019) 499-510. https://doi.org/10.1016/j.molstruc.2018.10.010.

28. M. Minteguiaga, E. Dellacassa, M.A. Iramain, C.A.N. Catalán, S.A. Brandán, A structural and spectroscopic study on carquejol, a relevant constituent of the medicinal plant Baccharis trimera (Less.) DC. (Asteraceae), J. Mol. Struct. 1150 (2017) 8-20. https://doi.org/10.1016/j.molstruc.2017.08.068 .

29. F. Chain, M.F. Ladetto, A. Grau, C.A.N. Catalán, S.A. Brandán, Structural, electronic, topological and vibrational properties of a series of N-benzylamides derived from Maca (*Lepidium meyenii*) combining spectroscopic studies with ONION calculations, J. Mol. Struct. 1105 (2016) 403-414. https://doi.org/10.1016/j.molstruc.2015.10.082.

30. H. Abdelmoulahi, H. Ghalla, S. A. Brandán, S. Nasr, Structural study and vibrational analyses of the monomeric, dimeric, trimeric and tetrameric species of acetamide by using the FT-IR and Raman spectra, DFT calculations and SQM methodology, *J. Mater. Environ. Sci.* (JMESCN) 6 (11) (2015) 3094-3109.

31. F. Chain, E. Romano, P. Leyton, C. Paipa, C.A.N. Catalán, M.A. Fortuna, S.A. Brandán, An experimental study of the structural and vibrational properties of sesquiterpene lactone cnicin using FT-IR, FT-Raman, UV–visible and NMR spectroscopies, *J. Mol. Struct.* 1065-1066 (1) (2014) 160-169. https://doi.org/10.1016/j.molstruc.2014.02.057 .

32. F.E. Chain, P. Leyton, C. Paipa, M. Fortuna, S.A. Brandán, FT-IR, FT-Raman, UV-Visible, and NMR spectroscopy and vibrational properties of the labdane-type diterpene 13-epi-sclareol, *Spectrochim. Acta Part A.* 138 (2015) 303-313. https://doi.org/10.1016/j.saa.2014.11.0499

33. E. Romano, A.B. Raschi, A. Benavente, S.A. Brandán, Structural analysis, vibrational spectra and coordinated normal of 2R-(−)-6-hydroxytremetone, Spectrochim. *Acta A Mol. Biomol. Spectrosc*. 84 (2011) 111– 116. https://doi.org/10.1016/j.saa.2011.09.011 .

34. A.B. Nielsen, A.J. Holder, Gauss View 3.0, User's Reference, GAUSSIAN Inc., Pittsburgh, PA. 2000–2003.

35. S. Miertus, E. Scrocco, J. Tomasi, Electrostatic interaction of a solute with a continuum. Chem. Phys. 55 (1981) 117–*129.* https://doi.org/10.1016/0301-0104(81)85090-2 .

36. J. Tomasi, J. Persico, Molecular Interactions in Solution: An Overview of Methods Based on Continous Distributions of the Solvent, Chem. Rev. 94 (1994) 2027-2094. https://doi.org/10.1021/cr00031a013

37. A.V. Marenich, C.J. Cramer, D.G. Truhlar, Universal solvation model based on solute electron density and a continuum model of the solvent defined by the bulk dielectric constant and atomic surface tensions, J. Phys. Chem. B113 (2009) 6378-6396. https://doi.org/10.1021/jp810292n .

38. M.J. Frisch, G.W. Trucks, H.B. Schlegel, G.E. Scuseria, M.A. Robb, J.R. Cheeseman, G. Scalmani, V. Barone, B. Mennucci, G.A. Petersson, H. Nakatsuji, M. Caricato, X. Li, H.P. Hratchian, A.F. Izmaylov, J. Bloino, G. Zheng, J.L. Sonnenberg, M. Hada, M. Ehara, K. Toyota, R. Fukuda, J. Hasegawa, M. Ishida, T. Nakajima, Y. Honda, O. Kitao, H. Nakai, T. Vreven, J.A. Montgomery, Jr., J.E. Peralta, F. Ogliaro, M. Bearpark, J.J. Heyd, E. Brothers, K.N. Kudin, V.N. Staroverov, R. Kobayashi, J. Normand, K. Raghavachari, A. Rendell, J.C. Burant, S.S. Iyengar, J. Tomasi, M. Cossi, N. Rega, J.M. Millam, M. Klene, J.E. Knox, J.B. Cross, V. Bakken, C. Adamo, J. Jaramillo, R. Gomperts, R.E. Stratmann, O. Yazyev, A.J. Austin, R. Cammi, C. Pomelli, J.W. Ochterski, R.L. Martin, K. Morokuma, V.G. Zakrzewski, G.A. Voth, P. Salvador, J.J. Dannenberg, S. Dapprich, A.D. Daniels, O. Farkas, J.B. Foresman, J.V. Ortiz, J. Cioslowski, and D.J. Fox, Gaussian, Inc., Wallingford CT, 2009.

39. P. Ugliengo, Moldraw Program, University of Torino, Dipartimento Chimica IFM, Torino, Italy, 1998.

40. B.H. Besler, K.M. Merz Jr, P.A. Kollman, Atomic charges derived from semiempirical methods, *J. Comput. Chem.* 11 (1990) 431-439. https://doi.org/10.1002/jcc.5401104044

41. G. Keresztury, S. Holly, G. Besenyei, J. Varga, A.Y. Wang, J.R. Durig, Vibrational spectra of monothiocarbamates-II. IR and Raman spectra, vibrational assignment, conformational analysis and *ab initio* calculations of *S*-methyl-*N,N*-dimethylthiocarbamate, *Spectrochim. Acta,* 49A (1993) 2007-2026. https://doi.org/10.1016/S0584-8539(09)91012-1

42. D. Michalska, R. Wysokinski, The prediction of Raman spectra of platinum(II) anticancer drugs by density functional theory, Chem. Phys. Lett. 403 (2005) 211-217. https://doi.org/10.1016/j.cplett.2004.12.096

43. R. Ditchfield, Self-consistent perturbation theory of diamagnetism. I. A gage-invariant LCAO (linear combination of atomic orbitals) method for NMR chemical shifts, Mol. Phys. 27 (1974) 714–722.

44. R.A. Rudyk, M.A. Checa, C.A.N. Catalán, S.A. Brandán, Structural, FT-IR, FT-Raman and ECD spectroscopic studies of free base, cationic and hydrobromide species of scopolamine alkaloid, J. Mol. Struct.1180 (2019) 603-617. https://doi.org/10.1016/j.molstruc.2018.12.040 .

45. S.A. Brandán, Understanding the potency of heroin against to morphine and cocaine, *Ijsrm. Human.* 10 (2) (2018) 97-140.

(2019) ; http://www.jmaterenvironsci.com